Pirani pressure sensor with distributed temperature measurement

B.R. de Jong, W.P.Bula, D. Zalewski, J.J. van Baar and R.J. Wiegerink
MESA+ Research Institute, University of Twente
P.O. Box 217, NL-7500 AE Enschede, The Netherlands
e-mail: b.r.dejong@utwente.nl fax: +31 53 4893343

Abstract

Surface micro-machined distributed Pirani pressure gauges, with designed heater-to-heat sink distances (gap-heights) of 0.35 μm and 1.10 μm, are successfully fabricated, modeled and characterized. Measurements and model response correspond within 5 % of the measured value in a pressure range of 10 to $2*10^4$ Pa. The distributed nature of the sensor facilitates pressure measurement to be independent of the Temperature Coefficient of Resistance of the resistors. This also provides an inherent compensation for heat loss via the membrane supporting the heater, extending the lower pressure range.

Keywords

pressure sensors, Pirani sensors, thermal sensors, distributed sensing

INTRODUCTION

In Pirani pressure sensors, use is made of the Pirani-effect. In short, this is the effect occurring when the gap-height and the mean free path of the gas are in same range causing the apparent thermal conductivity of the gas to be dependent on the pressure. Large-scale Pirani sensors are used frequently to measure very low pressures, but for higher pressures smaller gaps are needed. These gaps can be much reduced and accurately fabricated with the help of surface micro machining.

Recently, a distributed Pirani pressure gauge with a gap of 1.0 μm and a circular membrane was presented [1, 2]. The gap is now further reduced, using a thin poly-silicon sacrificial layer, which makes the sensor suitable for higher pressures. Furthermore, a rectangular membrane was used instead of a circular one. The latter significantly simplifies measurement of the temperature distribution, and also a much simpler one-dimensional model can be used. Several membrane sizes were fabricated, with a width of 100 μm and a length ranging from 100 to 450 μm. All membranes had a 15 μm wide ridge with a higher gap to reduce the heat transport to the silicon substrate. Figure 1 shows a photograph of a fabricated device.

Because of the introduced large width-length ratio of the membranes, the heat-conduction can be modeled along the membrane cross-section (see the line x-x' in Figure 1) with a one-dimensional model. The temperature profile along the cross-section varies with pressure. Measuring the temperature distribution instead of the average temperature of the membrane has two advantages: the measurement becomes independent of the Temperature Coefficient of Resistance (TCR) of the temperature sensing resistors and the heat loss to the substrate is implicitly taken in account, which extends the lower pressure range.

Sensors with different gap heights respond differently to a certain pressure (ratio of mean free path and gap-height is different). Combining measurements from different sensors allows elimination of the gas dependence of the sensor [3].

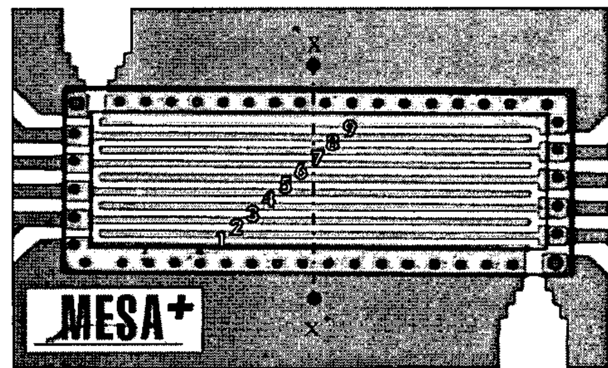

Figure 1. Picture of a distributed pirani sensor of 100 x 240 μm. Resistor segments are numbered from 1 to 9. Current is fed via the two thick wires. The other connections are used to measure the voltage over the resistor segments.

PRINCIPLE OF OPERATION

The silicon-rich silicon nitride (SiRN) membrane is heated via a current flowing through an integrated platinum resistor (see Figure 1, wires 1 to 9). Since the resistance is temperature dependent, the voltages over the resistor segments are a measure for the temperature. A temperature profile can be measured along the cross-section. The resistance as a function of the temperature rise ΔT [K] can be expressed as (1) (with α [K^{-1}] the TCR and R_0 [Ω] the initial resistance):

$$R(\Delta T) = R_0(1+\alpha\Delta T) \quad (1)$$

The temperature at a certain position on the membrane depends on the heat transport through the gap and through the membrane to the substrate. The thermal conductivity (G_{th} [W K^{-1}]) for heat transport through the gap depends on

the pressure and the type of gas or gas mixture and can be expressed by:

$$G_{th} = \frac{Q}{\Delta T} = \frac{\kappa A}{l} \tag{2}$$

Where ΔT [K] is the temperature difference between membrane and substrate, Q [W] is the heating power, κ [W K^{-1} m^{-1}] is the thermal conductivity of the medium, A [m^2] is the cross sectional area of the conductance and l [m] is the conductance length (the gap height in this case).

The temperature distribution along the membrane is modeled using an equivalent electrical lumped element model as shown in Figure 2.

The membrane and the gap are split up in segments, each having its own thermal conductance value. Application of heat power through the resistor segments is modeled by current sources. The temperature at each segment is the thermal equivalent of the voltage over the conductance elements.

Conductance through the gap is shown variable since it depends on the pressure, while membrane conductance is fixed. The conductance symbols are explained in Table 1.

The values of the rise in temperature ΔT of the heater segments can be calculated from the heating power and the conductance values with the following matrix equation:

$$\Delta T_j = [G]^{-1}{}_{jk} P_k$$

with,

$$[G] = \begin{bmatrix} \circ & \bullet & & & 0 \\ \bullet & \square & \bullet & & \\ & \ddots & \ddots & \ddots & \\ & & \bullet & \square & \bullet \\ 0 & & & \bullet & \circ \end{bmatrix} \qquad \begin{aligned} \circ &= g_b + g_{a3} + g_s \\ \bullet &= -g_m \\ \square &= 2g_m + g_a \end{aligned} \tag{3}$$

Table1. Explanation of conductance symbols

Conductance	Description
g_m	membrane conductance element
g_a	gap conductance element
g_b	membrane edge conductance element
g_s	membrane support conductance element
g_{a3}	edge gap conductance element

Where, j and k both range from 1 to 9. The power values P_k [W] are all equal to $(i^2 R_{el})/9$, with i [A] the current and R_{el} [Ω] the electrical resistance of the heater. The conductance elements can be calculated with equation 2. For the membrane elements, κ is equal to the thermal conductivity of SiRN. For the gap elements, κ is expressed by [4, 5]:

$$\kappa(P) = \tfrac{1}{3} \cdot n(P) \cdot \bar{v}(P) \cdot c^P \cdot \lambda(P) \tag{4}$$

Here $n(P)$ [m^{-3}] is the pressure (P [Pa]) dependent amount of molecules per unit volume, $\bar{v}(P)$ [m s^{-1}] is the mean velocity of the molecules, c^P [J K^{-1}] is the specific heat per molecule at constant pressure, and $\lambda(P)$ [m] is the mean free path of the molecules depending on the pressure. The mean free path can be approximated by [5]:

$$\lambda(P) = \frac{1}{\pi\sqrt{2}\sigma^2 n(P)} \tag{5}$$

With σ [m] the diameter of the gas molecule (rigid sphere model).

The thermal conductivity of a gas, as a material property, does not change with pressure, since the pressure dependence of n and λ cancels. However, in a narrow gap pressure sensor it appears to change because the gap height d [m] limits the mean free path [4].

Figure 2. Electrical lumped element model for the temperature distribution.

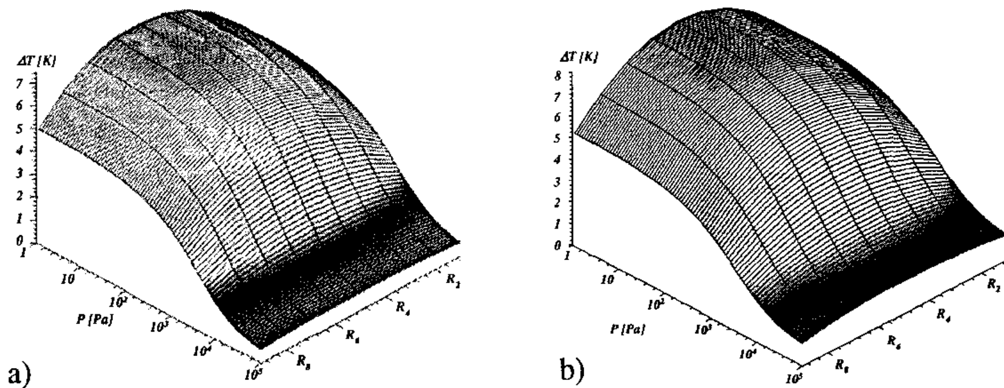

Figure 4. Result of the lumped element model; ΔT depending on the pressure and the position along the cross-section (Ri is resistor element i) for a gap of a) 0.35 μm and b) 1.1 μm. Heating current 1 mA.

The pressure dependence of the thermal conductance G_g [W K^{-1}], measured between the heater and heat sink in a Pirani pressure sensor can be described by the following expression [4]:

$$G_g = A_s \cdot K \cdot P \cdot \left(\frac{P_t}{P + P_t} \right) \tag{6}$$

Where A_s [m^2] is the effective surface area of the sensor, P_t [Pa] is the transition pressure that depends on the gap height d, and K [W/(K Pa m^2)] is a constant that depends on the type of gas and the accommodation effect. The latter accounts for the fact that an average molecule colliding with a surface does not fully reach thermal equilibrium with that surface. It can be shown that for a simple parallel-plate sensor configuration the transition pressure P_t is inversely proportional to the distance between the plates.

The dependence of the apparent thermal conductivity of nitrogen on the gap height and pressure is shown in Figure 3. For both curves three regions can be defined; molecular, viscous slip and viscous, which correspond to the linear, transition and horizontal part of the curve respectively. Lowering d shifts the pressure dependent part of the graph to higher pressures.

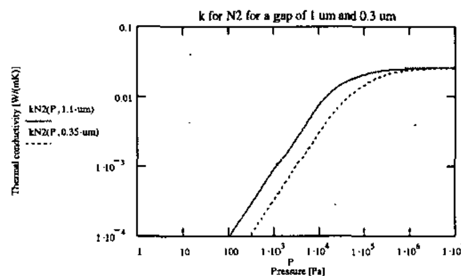

Figure 3. The apparent thermal conductivity of nitrogen for a gap height (d) of 1.1 μm (solid) and 0.35 μm (dashed).

Using the model to calculate the temperature rise at the nine resistor elements along the cross-section at different pressures, results in the graphs showed in Figure 4. The graph for a gap of 0.35 μm is shown in 4a) and that for 1.1 μm gap is shown in 4b). The current for the heating power is 1 mA.

FABRICATION PROCESS

A sacrificial polysilicon structure between two SiRN layers is etched away via etch-holes in the upper SiRN layer. In this manner rectangular SiRN membranes are realized with areas varying from 100 x 100 μm^2 to 100 x 450 μm^2.

A 15 μm wide ridge, with a higher gap, surrounds the membrane. This ridge reduces the heat transport through the membrane to the substrate. On the other hand, the effect of the distributed measurement is reduced. A trade-off should be made.

On top of the membrane, the resistor is integrated by lift-off of a 10 nm Cr adhesion layer and a 150 nm Pt layer.

The complete fabrication process is outlined in Figure 5. First a 0.5 μm thick layer of SiRN is deposited by LPCVD on a highly p-doped Si <100> wafer (a). Then, a 2 μm thick layer of polysilicon (forming the ridge) is deposited by LPCVD and structured (b).

A second layer of polysilicon is deposited by LPCVD and structured (c). This layer defines the gap height and is either 0.25 μm or 1.0 μm thick. Furthermore, 2.5 μm wide holes are etched to enable formation of little bumps during deposition of the second SiRN. These bumps serve as spacers (and surface reduction) to avoid sticking during the wet release of the membranes.

A third, 0.1 μm thick polysilicon layer is deposited and structured to define the height between the bumps and the substrate (d). The polysilicon is etched from the backside (front side protected by photo-resist) and a 1 μm thick layer

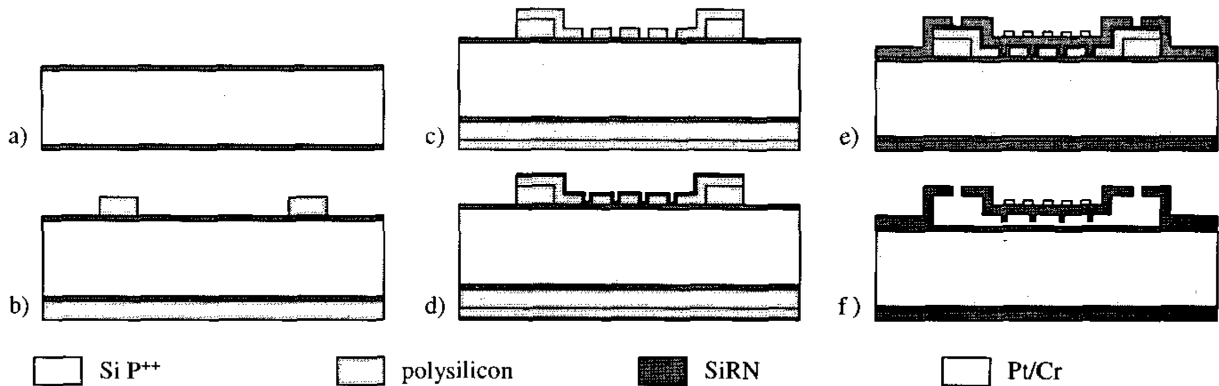

Figure 5. Fabrication process; deposition of SiRN (a), deposition and structuring of first layer of polysilicon (ridge formation) (b), deposition and structuring of second polysilicon layer (defining gap and "bump-mould") (c), deposition and structuring of third polysilicon layer (defining bump height) (d), etching polysilicon from backside, deposition and structuring of second SiRN layer and lift-off of platinum (e), wet release of the membrane (f).

of SiRN is deposited by LPCVD and structured, followed by a lift-off of platinum for the resistor (e).

Finally, the sacrificial polysilicon is etched away from under the SiRN membrane via the etch-holes by wet etching in either KOH or TMAH(f).

Due to tensile stress in the SiRN membrane, the membranes are slightly curved after release, as illustrated in Figure 6 [6]. This curvature is caused by the relatively high ridge around the membrane and the size of the membranes. Larger membranes or a higher ridge result in a stronger curvature.

Because of the curvature, the gap heights are slightly larger than the designed values. This is taken into account in the comparison with the model response..

MEASUREMENTS

Voltage was measured over the segments at various current and pressure (< 1 bar) values. The resistance values $R_j(i, P)$ for the segments 1 to 9 where derived. The rise in voltage $\Delta V_j(i,P)$ [V] was determined with the help of equation (1). In order to do this, the resistance values $R_{0,j}$ of the segments were needed. These are determined by extrapolation. Since $R(i)$ at a constant pressure is approximately linear for values of i in the mA-range, this is acceptable. When ΔT of equation (2) is inserted in equation (1), the following equation for $R(i)$ can be derived:

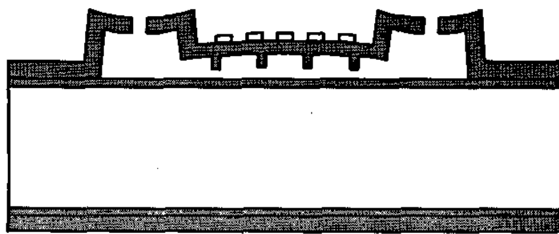

Figure 6. Curvature of the membrane due to the combination of tensile stress and the high ridge.

$$R(i) = R_0(1+\alpha i^2 R(i) R_{th}) \Rightarrow R(i) = \frac{R_0}{1-\alpha i^2 R_{th} R_0} \tag{7}$$

Where R_{th} is the reciprocal of G_{th} of equation (2) and $i^2R(i)$ is inserted for Q in equation (2).

The measured temperature rise and the temperature rise predicted by the model are normalized and plotted in Figure 7. Curves and measurements are shown for resistance segments R_5, R_7, R_9 and for both gap heights. The normalized temperature rise is defined as $\Delta T/(\Delta T)_{max}$.

Measured values are depicted as points, while the result of the model is shown by a continuous curve. The latter is solid for the gap of 1.1 μm and dashed for 0.35 μm; which is also shown by the labels in the graph.

Parameters to fit the model were K and P_t of equation (6), and d for the gap height and for the ridge height. d is used as a fitting parameter, because of the curvature of the membranes noted before.

Figure 7 shows, correspondence between the model and the measured values is within 5 percent in a pressure range of 10 to $2*10^4$ Pa. There clearly is a temperature gradient along the membrane cross section, which also follows nicely form the lumped element model. Curves of the segments R_7 and R_9 for the one gap do not start at the same values (for the low pressure range) as those of the other gap. This is caused by the difference in the values for the initial resistance R_0, which are not exactly equal for the segments and are not eliminated in the normalization.

The model results are plotted beyond the measurement points to verify the behavior for higher pressures than 1 bar. At these pressures the conductance through the gap approaches its limit. Firstly, the curves show this happens at two different levels for the different gap heights and secondly the curves for the resistor segments do not level at the same height.

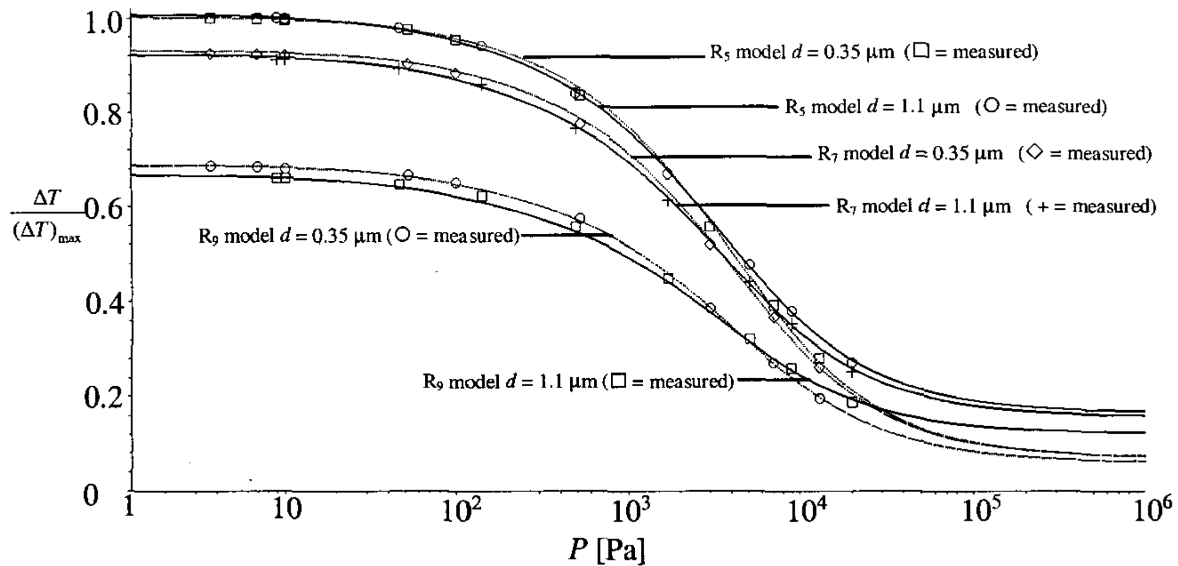

Figure 7. Temperature rise ΔT along the cross section of the membrane as a function of the pressure, normalized to the maximum ΔT for each gap height. Measurements are shown as points, model results as curves. The solid and dashed curves correspond to d = 1.1 μm and d = 0.35 μm respectively.

For high pressures ΔT becomes constant. This is caused by the fact that the conductance through gap is limited for high pressures. That conductance should be higher for the small gap than for the large gap. This is in correspondence to the plots. The ratio is roughly 2.

When the conductance due to the membrane and the gap is seen as two resistors in parallel, it is possible to find bounds for the ratio. If the conductance is defined by the membrane, the lower bound is 1. If on the other hand the conductance is defined by the gap, the upper bound would be equal to the ratio of the gap heights, which is about 3.

Conductance through the gap is limited, so at a certain high pressure a lumped element circuit, like in Figure 2, with fixed conductance in the gap can represent the sensor. From this representation follows, that in case of a limited gap conductance there will remain a temperature gradient along the membrane. This can be seen from the fact that the curves for different resistance segments do not level at the same ΔT.

CONCLUSIONS

Distributed Pirani pressure sensors with gap heights of 0.35 μm and 1.1 μm and large width-length ratio have been successfully realized in surface micromachining. SiRN membranes have been released via etching of a sacrificial gap defining structure of polysilicon.

An electrical lumped element model for the temperature profile along the cross section of the distributed sensor is developed. This model is based on analogy between current and heat power flow through a circuit of electric and thermal resistances, respectively.

Measurements have been performed in order to determine the voltage rise along the membrane cross section as a function of the pressure. The lumped element model corresponds within 5 percent in a range of 10 to $2*10^4$ Pa.

Additional characterization at pressures above 1 bar needs still to be done.

REFERENCES

[1] J.J. van Baar, R.J. Wiegerink, T.S.J. Lammerink, J.W. Berenschot, G.J.M. Krijnen, M.C. Elwenspoek, "Combined Pirani/bending membrane pressure sensor", MEMS, Las Vegas, January 20-24, 2002.

[2] J.J. van Baar, R.J. Wiegerink,J.W. Berenschot, T.S.J. Lammerink, G.J.M. Krijnen, M.C. Elwenspoek, "Pressure sensor based on distributed temperature sensing", IEEE Sensors'02, Orlando, June 11-14, 2002.

[3] U. Bonne, and D. Kubisiak, "Burstproof, thermal pressure sensor for gases," Solid State Sensor and Actuator Workshop, Hilton Head, South Carolina, June 13-16, 1994, pp. 78-81.

[4] J.J. van Baar, "Distributed Thermal Micro Sensors for Fluid Flow", PhD-thesis, University of Twente, 2002, pp. 41-44.

[5] J.O. Hirshfelder, C.F. Curtiss, R.B. Bird, "Molecular Theory of Gasses and Liguids" 2nd edition, John Wiley & Sons Inc., 1963.

[6] B.R. de Jong, "Fabrication, modeling and characterization of test devices for a high frequency power sensor", MSc-thesis, University of Twente, 2002.